MEASUREMENT AND CONTROL SYSTEM DESIGN FOR PROPELLER-WING SYSTEM EXPERIMENTS

Wang Wei[1], Zhang Zhitao[2], Xie Changchuan[1,3], Yang Chao[1,3], Huang Kunhui[1]

[1]School of Aeronautic Science and Engineering, Beihang University, Beijing 100191, China
wwase@buaa.edu.cn
xiechangc@buaa.edu.cn
yangchao@buaa.edu.cn
hkk2333@buaa.edu.cn

[2]China Research and Development Academy of Machinery Equipment, Beijing, 100089, P.R. China
zhangzhit1605@buaa.edu.cn

[3]Hangzhou International Innovation Institute, Beihang University, China

Keywords: Propeller-wing system, wind tunnel experiment, measurement and control system, data acquisition

Abstract: An integrated measurement and control system suitable for ground and wind tunnel testing of a distributed propeller-wing system was designed. The real-time measurement, recording and display of several indicators including the propeller aerodynamic load, wing root load, propeller rotation speed, wing structural deformation and wing surface pressure during the experiment were obtained by using a six-component balance, an optical sensor, a data acquisition device and graphic display. Computer software was also utilized to process the collected test data, which were then compared with the numerical simulation results to verify the effectiveness and reliability of the measurement and control system. Results of high-precision computational fluid dynamics (CFD)/computational structural dynamics (CSD) aeroelastic simulations and Nastran SOL144 calculations used in this study are collected. In terms of vertical displacement of the wing tip and wing deformation distribution tested during the experiment. It is observed that the simulation results obtained in this study are in consistency with the results of wind tunnel tests using commercial software, proving the effectiveness of the experiment design.

1 INTRODUCTION

With the promotion of energy conservation, environmental protection, and the advent of the electric era, propeller aircrafts have received increasing attention from the aviation industry. Aerodynamic interference between propeller and wing has become a research hotspot [1-3]. Slipstream induced by the propeller can lead to complicated aerodynamic interference, altering the flow field of the wing, tail, and other lifting surfaces of the aircraft. As a result, it influences the aerodynamic characteristics of the aircraft, or even its controllability and stability under severe circumstances. The slipstream effect of the propeller significantly affects the load distribution and structural deformation of the aircraft wing [4,5]. Wing deformation in turn alters the flow field of the propeller. Thus, the aeroelasticity issues introduced by a propeller-wing coupling system cannot be ignored. Especially for a distributed propeller aircraft, the wing is affected more greatly

by the distributed slipstream. The aeroelastic response and stability of the wing is highly sensitive to the distributed slipstream.

In previous research, CFD [6], viscous vortex particles [7], the surface element method [8], and the blade element method [9] were used to aerodynamically model the wing and the propeller. In addition, ground test and wind tunnel test were also conducted to investigate this complex aerodynamic phenomenon [10]. Conclusions have been made that propeller-wing interactions partially account for this interference.

As is universally known, wind tunnel testing stands as one of the most pivotal validation methods in aerospace engineering. Compared with conventional aircraft wind tunnel test, propeller-wing coupled system is featured with significant aerodynamic interference between propeller and wing, and such interference will in turn affects the aeroelastic characteristics of the coupled system. Zhang Xingyu et al. [11] analyze the aero-propulsion coupling characteristics of a distributed electric propulsion aircraft through wind tunnel testing. In the experiment, a six-component balance is used to obtain the thrust of propeller, the lift of wing, and the drag of wing. The result shows that both lift and drag coefficients increase after electric ducted fans (EDFs) are installed on the trailing edge of the wing, compared with a clean wing. Moreover, it is possible to reduce the drag while keeping the lift unchanged by reducing the wing area. Shreyas et al. [12] use particle image velocimetry (PIV) measurements to reveal details about the propeller-wing interactional aerodynamics and the flow field. It is found that interactions between the propeller and the wing resulted in significant flow characteristics. However, a large volume of measurement and control system for ground and wind tunnel experiment of propeller-wing system often focuses on the lift and drag characteristics of a rigid wing only, but little attention is paid to the issues of structural vibration and multi-factor coupling of an elastic wing. Therefore, it is necessary to conduct experiments on the effect of propeller slipstream on the aerodynamic and aeroelastic characteristics of elastic wings. Furthermore, designing a good measurement and control system is important to obtain the data of such complex system in various states systematically and comprehensively through wind tunnel testing.

In the presented work, the force balance and pressure sensors are most widely used to measure the aerodynamic loads and surface pressure distribution of the wing in any wind tunnel test setup. For a propeller-wing system, force balances are also mounted to measure the thrust of each propeller. An advanced Fiber Bragg Gratings are used to obtain the strain distribution on the wing and then the data are used to recovery the value of wing deflection [13,14]. Rotation tachometers are used to detect the speed of propellers in real time, single-axis accelerometers are installed to assist in precision structural vibration measurement. The PCI eXtensions for Instrumentation (PXI) platform and other dedicated measuring devices are employed to build a multi-state comprehensive monitoring system for sensors. A custom controller module is designed to simplify the controlling of multiple motors, thus optimizing the workflow for rapid repeating experiments in multiple operating conditions (consisting of a large number of parameter combinations).

This paper is organized as follows: The background information of the experiment is introduced in Section 1. Detailed descriptions of the experiment setup are presented in Section 2. Section 3 discusses major issues encountered during the experiment, and Section 4 provides test results and makes conclusions.

2   EXPERIMENT SETUP

In the construction of a measurement and control system, the primary task is to clarify the measurement and control objects of the ground/wind tunnel test. For the propeller-wing coupling system test, following measurements should be made. Designing of the measurement and control system is shown in Fig. 1.
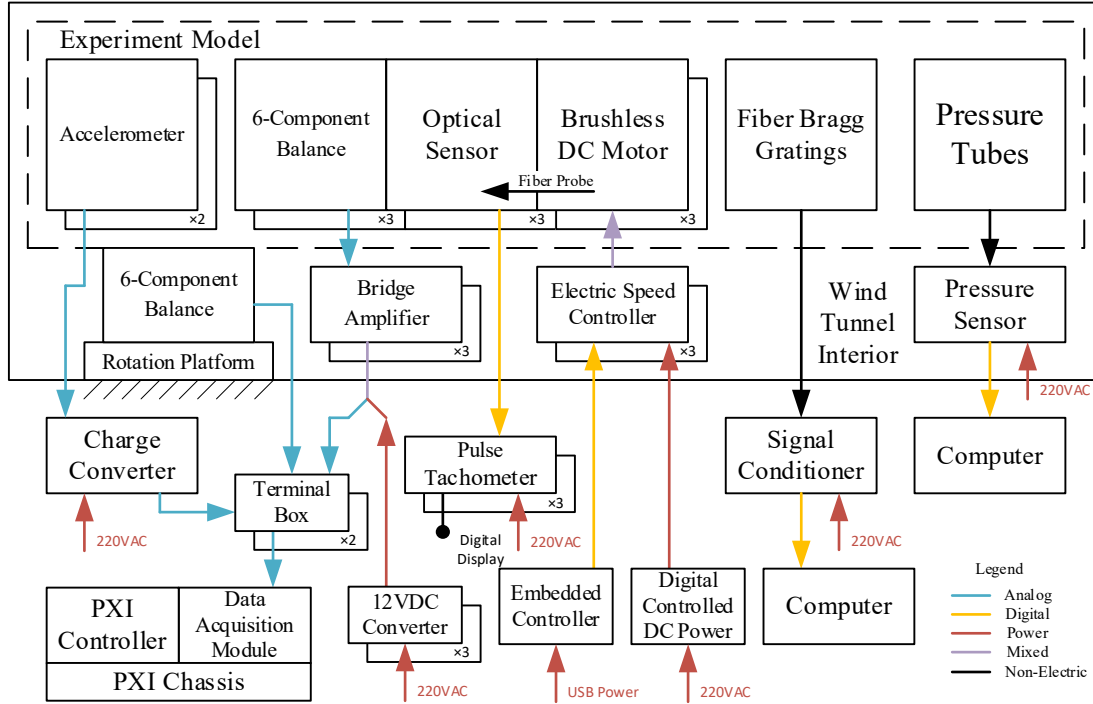
Figure 1: Block diagram of the measurement and control system

2.1   Propulsion Measurement

In this part of measurement, the rotational speed and aerodynamic load of the propeller are measured. Photoelectric reflection sensors are performed to measure the rotational speed of propeller. The sensor consists of a light transmitter diode, a receiver diode and an adjustable threshold triggering circuit with hysteresis. It inverts the output signal when the reflected light level rises above the high threshold and restores the output signal when the reflected light level falls below the low threshold. Optical fibers are connected to the transmitter and receiver at one end and points at the measured target through a micro-size optical probe on the other end. In this way, the light path is concentrated and the installation of the system is simplified. Shown in Fig. 2, each probe is embedded close to the motors on surface of the wing shell and points at the root of the propellers. White tape is applied at one root of the propeller, causing high reflection that can be recorded by the reflection sensor during each rotation. During the construction of the experiment setup, high and low thresholds of each sensor are adjusted so that only one pulse is generated when the propeller root with white tape sweeps through it. In this way, sensor detection failure or the generation of multiple pulses by the sensor per rotation can be effectively prevented. The generated pulse signal is then sent to a pulse capture and process tachometer with segment display, which directly indicates the propeller speed to operators.
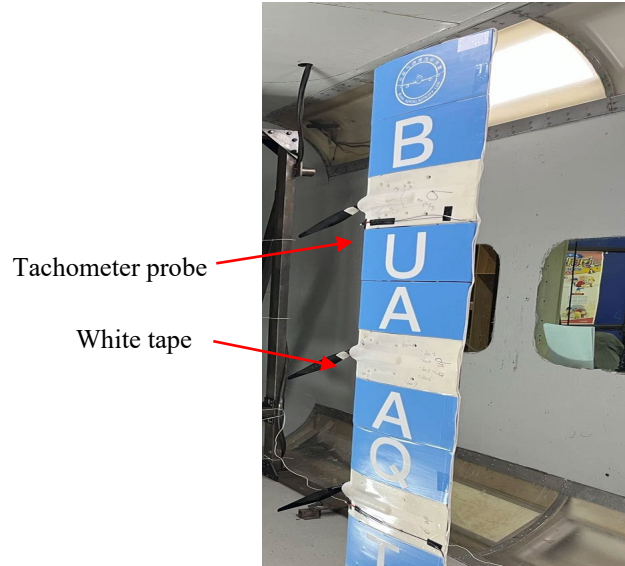
Figure 2: Photo of the test model in propeller-elastic wing configuration

The aerodynamic load of the propeller is measured using a six-component strain gauge force balance, which also serves as a part of the structural connection between the main beam of the wing and the motor-propeller assembly, as shown in Fig 3. All forces and moments applied to the motor, including gravity, the thrust of the propeller and motor-propeller torque, are measured by the balance under this configuration. The force balance utilizes the full Wheatstone bridge to minimize errors induced by high temperature variations generated by the motor, and outputs differential analog voltage signals consisting of three-axis forces and moments of the motor-propeller assembly. Instrumentation amplifier circuits are ground-shielded and connected to the single-ended analog to digital converter (ADC) channels on the data acquisition (DAQ) module of the PXI system for amplifying, converting, and fine-tuning these outputs to single-ended analog voltage signals. The DAQ module has 16 differential or 32 single-ended analog input channels with 16-bit resolution and 250kS/s maximum sampling speed. The input range of each channel is set to ±0.2V, ±1V, ±5V or ±10V. Since the frequencies of interest for this experiment are under 200Hz, the sample speed is set to 1kS/s for all channels, which will give the measuring system adequate settling time to high accuracy. The converted digital data is transmitted to the embedded computer on the PXI platform for measuring and recording the aerodynamic loads on the motor-propeller assembly.
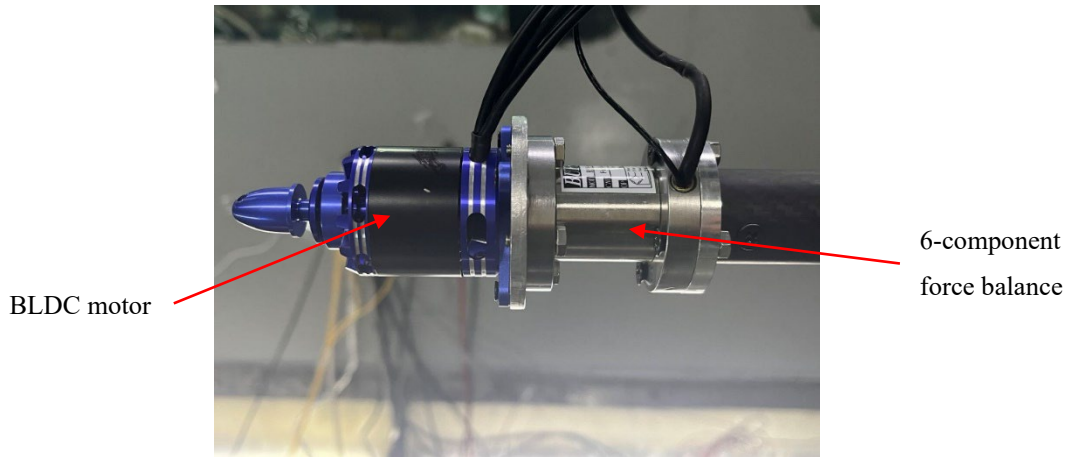
Figure 3: Photo of the motor and the balance

2.2 Aerodynamic Measurement of the Wing

In this part, the pressure distribution on the wing surface and loads on the wing root are measured.

The pressure distribution on the wing surface is detected by pressure taps, which are connected to dynamic pressure sensors via hoses, as demonstrated in Fig. 4. Pressure taps are distributed both inside and outside the slipstream affected zones in order to study propeller interference with wing aerodynamic distribution. Sensor arrays are utilized to collect pressure data, which are then sent to a dedicated computer for monitoring and recording.
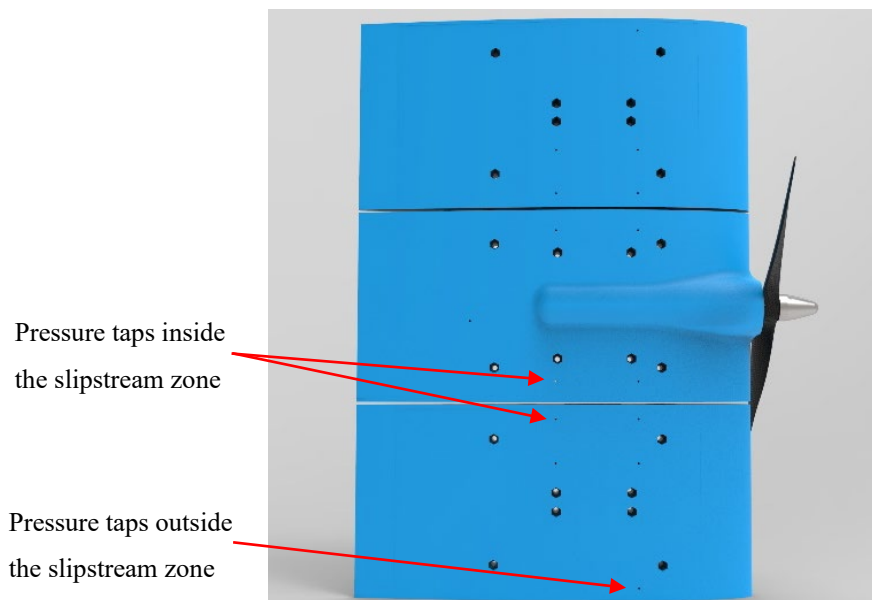

Figure 4: Partial 3D diagram of the wing

The whole wing structure is installed on a carbon-fiber main beam, which is clamped to a six-component force balance fixed on the rotation platform of the wind tunnel. This balance measures the overall load of the wing. The wing is installed vertically in the wind tunnel to minimize deformation at static state and to concentrate the influence of gravity on the vertical axis so that no other forces or moments are introduced and require measuring in the ideal case. Complete

experiment model in the wind tunnel after installation is presented in Fig 5. The force balance outputs six-channel differential voltage signals generated by the Wheatstone bridges which are connected directly to 6 differential ADC channels on the DAQ module of the PXI system without amplification. However, it introduces signal quality issues, which will be discussed later.

Figure 5: Wing installed in the wind tunnel

2.3   Structural Measurement

In the structural measurement of the wing, the deformation distribution on the wing and wing tip acceleration are measured. Wing structural design and modelling is centered on a carbon fiber main beam. 3D printed shells form the structrual support of the aerodynamic surface, as partially shown in Fig 2. These shells are devided into 11 sections with 2mm gaps along the wingspan to minimize their impact on structural additional rigidity. Fixture is designed to clamp the wing structure onto the total force balance installed on the rotation platform.

The deformation of the wing structure is measured by fiber Bragg grating sensors. A fiber Bragg grating is a type of distributed Bragg reflector constructed in a short segment of the optical fiber that reflects particular wavelengths of light and transmits all the others. Optical fiber deformation leads to a periodic change of the microstructure and the Bragg wavelength, thus altering the wavelength being reflected to optical sensors for strain measurement. Each fiber contains multiple Bragg gratings, which are adhered to multiple points on the carbon fiber beam for strain distribution measurement. Light signals in these light fibers are manipulated and converted to electrical signals through a signal conditioner and output to a dedicated computer. Restoring wing deformation can be achieved using measured strain data and software algorithms.

Two accelerometers are used to measure wing tip vibrations. Charge signals generated by the accelerometers are sent to a charge-to-voltage converter, which is connected to 2 single-ended ADC channels on the DAQ module of the PXI system.

2.4   Control Module

In a distributed propeller-wing system, the independent control of the rotation speed of the distributed propeller is necessary to the simulation of the required speeds for various test conditions.

A dedicated motor control module is designed for this purpose. The module is based upon an embedded controller chip that simplifies the development procedure. The module generates pulse width modulation (PWM) signals that configure electronic speed controller for each motor, PWM settings are visualized through three lines of digital display, corresponding to the first 4 digits of

each line in Fig. 6. An integrated operating interface with rotary encoder and buttons simplifies the procedure for rapid adjustment of the motor speed.
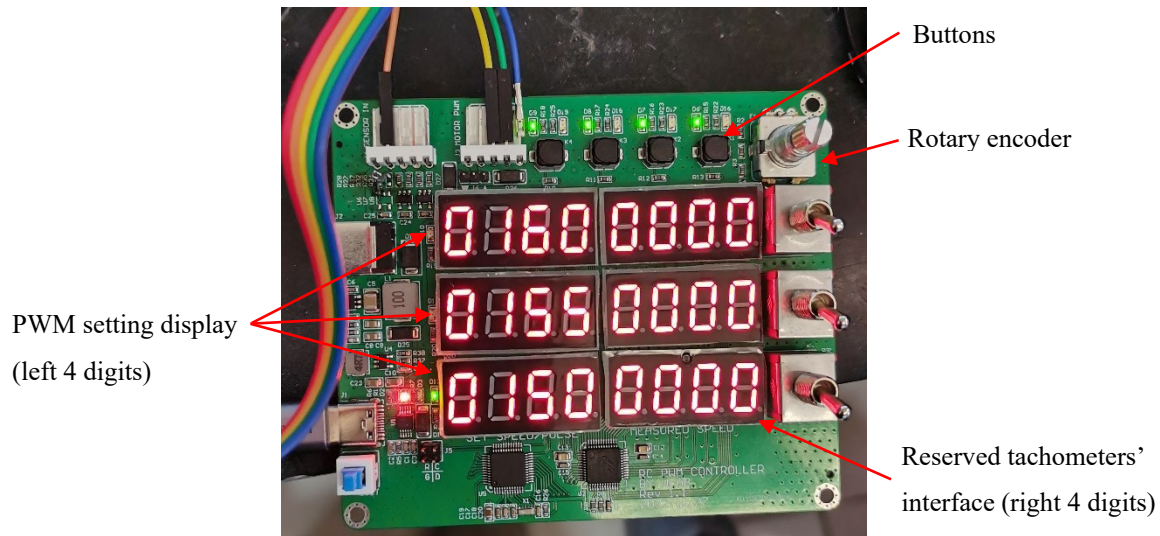

Figure 6: Photo of the control module

3 EXISTING PROBLEMS AND SOLUTIONS

3.1 Static Testing

Due to assembly errors in the test model, gaps generated by vibrations, and fluctuations in ambient temperature, the data measured by sensors can drift significantly within the timespan of the experiment. In addition, crosstalk between signal lines and power supply lines during the experimental process reduces the reliability of test data and increases zero offset errors. Therefore, it is imperative to conduct static testing before each experiment to correct these errors to the maximum extent. Specifically, the static data from various sensors of the assembled test model are collected before the experiment begins. Through analyzing these data, it is possible to detect whether there is any signal interference in the testing system and whether the signal shielding is adequate. During wind tunnel tests, it is necessary to collect static data after the incoming flow becomes stabilized and before the motor starts to work (when the incoming flow velocity and angle of attack change with time). These static data provide the zero positions of various sensors at different flow velocities and angles of attack, serving as a reference for the changes in test data under the influence of propeller coupling after the engine starts. In this study, 10 seconds of static data are collected as required.

3.2 Electrical Signal Quality

Electrical signal quality is critical for measuring data that reflect frequency responses especially in wind tunnel experiments considering dynamic aeroelasticity. In the experiment model, there are 38 discrete signal wirings that can be accessed outside the wind tunnel. These wirings consist of 20 single-ended analog wires with 10 volts peak to peak, 6 pairs of differential analog wires with millivolt-level output, 3 single-ended digital wires constantly transmitting pulse-width modulation signals at 50hz, and 3 single-ended digital wires transmitting variable frequency pulses depending on the propeller speed. Wiring and tubing can be seen in Fig. 7. For both the single-ended and differential analog wires, the sample speed of 1kS/s is adopted. The longest wirings (up to 4 meters)

connect the sensors at the wing tip with the measuring devices inside the wind tunnel control room. Therefore, signal crosstalk and ambient electromagnetic noise severely interfere measured signals during setup adjustment and testing. Metal foil is electrically connected to the metal wall of the wind tunnel isolate and shield the analog wires. Frequency spectrum analysis of the recorded vibration data shows no observable spike at 50hz, and the spectrum only peaks near computed modal frequencies and propeller rotation frequencies. The results prove the effectiveness of noise reduction.
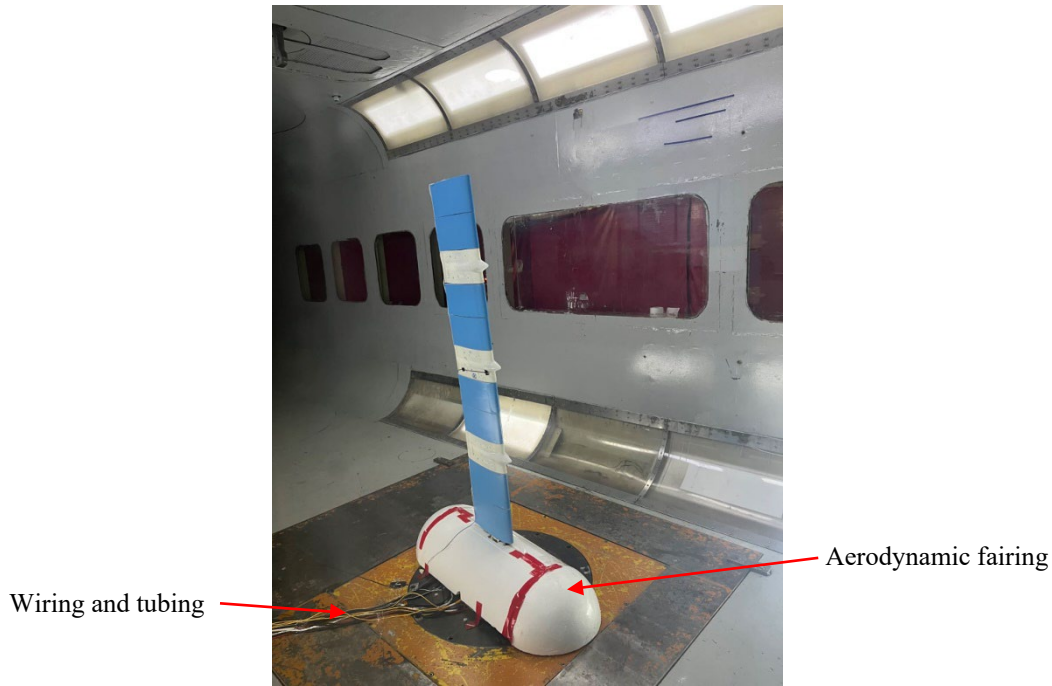

Figure 7: Experiment model during wind tunnel test (clean wing configuration)

Another technique to improve signal quality is to amplify the sensor signal before it is transmitted to data acquisition devices. The Wheatstone bridge circuit used inside the force balance of the propulsion system outputs a pair of differential signals that generate ±20mV differential voltage at full scale, and the signals are severely interfered by microvolt-level noise. An amplifier circuit should be placed as close as possible to the sensor, thus reducing the possibility that weak signals are exposed to noise without introducing extra inertia or aerodynamic components to the test model. During the construction of the test model, multiple amplifier modules shielded with grounded metal casings and other electronics in the wind tunnel are installed inside a faring at the bottom of the model, presented in Fig. 7. The faring simulates the fuselage of the aircraft, protecting devices inside the wind tunnel while minimizing their influence on the flow field. These amplifier modules are provided with instrumentation amplifiers with a gain value of 250, which lift the output amplitude to ±5V while greatly reducing internal resistance of a signal source. Both can increase signal resistivity to electromagnetic noise.

However, force balances installed in the wind tunnel for the measurement of the overall load of the wing are not provided with any amplifier circuit. Since wind tunnel tests mainly focus on static load, and a low-pass filter of 4Hz is installed in the DAQ module for reducing noise to the level of precision required by these scenarios, signal quality issues are not considered in this study even if the millivolt-level signal of the balance is connected directly to the DAQ module. Nevertheless,

the wind tunnel experiment requires the acquisition of dynamic responses up to 200Hz, so the use of this low-pass filter will obviously depress information of interest. To solve the problems, the input range of the corresponding analog input channel is set to ±0.2V, which can help minimize bit loss. In addition, shielded twisted pairs are used to wire the differential signal of the balance, and most noise generated by electromagnetic fields is converted into common-mode signals, which in theory are cancelled as the wiring is connected to differential channels on the DAQ module. During the experiment, common-mode noise in the DAQ module can reach 10 volts if there is no proper shielding. The DAQ module has a common-mode rejection ratio (CMRR) of 92dB, indicating that about 0.25mV of noise is introduced to the acquired data. The noise analysis reveals that further investigation on signal quality is needed to improve the reliability of this experiment.

3.3   Speed Measurement and Throttle Control

Current configuration for propeller speed measurement utilizes reflective optical tachometer. While this type of sensor provides adequate performance throughout the experiment procedure, it exhibited drawback in robustness due to airflow interruption, structural vibration and distance uncertainties in probe installation during the experiment, resulting in frequent calibration required for sensor thresholds and probe direction, increasing time consumption for every experiment cycle. Solutions to this issue include using hall effect sensor installed to the aft part of the motor that can steadily detect changes in the motor's magnetic field during rotation for precision speed measurement, or using grating rotary encoder installed onto the motor shaft for better robustness and improved precision.

During designing period of the controller module, connector interface is reserved for the tachometers. The purpose for this interface is to enable hardware-in-the-loop throttle control capability on this module. Visual interface for tachometer readings is also reserved, corresponding to the last 4 digits of each line in Fig. 6. However, this function was not implemented due to time limitations. Throttle had to be controlled man-in-the-loop through tachometer readings during the experiment, creating two major problems. One is that internal resistance of the power cable for the motors can lead to power drop at high current, and current consumption is directly related to throttle, causing speed changes on other motors when adjusting throttle for one motor. The other is that incoming airflow in the wind tunnel can also interfere propeller speed to a lesser extent. These issues led to frequent adjustment on throttle during practical operation, and can be better handled if hardware-in-the-loop control is introduced.

4   RESULT ANALYSIS

Before conducting the wind tunnel experiment, ground tests for system stability and sensor reliability are carried out in laboratory environment. Thrust and torque data of the motors are gathered and compared to CFD simulation results. For both the experiment and simulation, the propeller speed is set at 6000 r/min and 7000 r/min, and the incoming flow velocity is set at 0 m/s. It represents the ideal ground condition. Fig. 8 presents the ground test results, the static thrust, and torque of the propeller are compared with the CFD simulation outcomes. It can be seen from the figures that the static thrust increases with the increase of the rotation speed, and higher difference occurs when the propeller rotational speed is 7000 r/min. The possible reason is that higher motor speed causes the heating of the balance, significant temperature fluctuations, and increased mechanical vibration. These factors should be considered during wind tunnel testing and data processing.
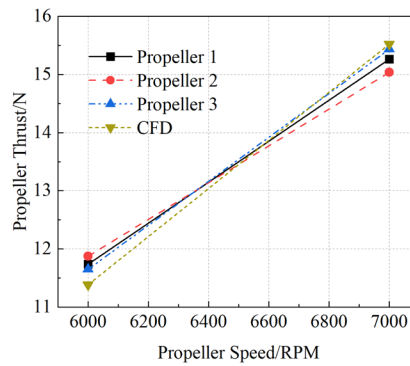
Figure 8: Static thrust experiment results of the distributed propellers compared with CFD simulation

The wind tunnel experiment was conducted at the FD-09 low speed wind tunnel of China Academy of Aerospace Aerodynamics. Fig. 9 depicts the spanwise distribution curve of deformation on the vertial direction under 3° angle of attack. Comparison shows high precision CFD/CSD numeric simulation result being slightly lower than results from wind tunnel test and commercial software, yet in general the numeric simulation results retain favorable consistency with wind tunnel test result from the structural static aeroelastic deformation point of view, proving the CFD/CSD method to be effective and accurate.
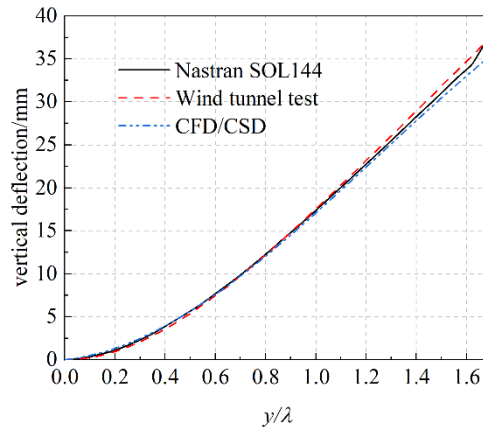

Figure 9: Comparison of test and simulation results of wing spanwise vertical deformation distribution under 3° angle of attack

Fig. 10 illustrates the static deformation of the wing tip as the angle of attack increases from 1° to 5° at an incoming flow velocity of 19 m/s during the wind tunnel experiment. The vertical displacement of the wing tip increases linearly with the increase of the angle of attack. At an angle of attack of 5°, the vertical displacement of the wing tip is approximately 3.76% of the span, indicating that the wing deformation is still linear. The high-precision CFD/CSD aeroelastic numerical simulation and Nastran SOL144 calculation results are also plotted in Fig. 10. Regarding the vertical displacement of the wing tip, the maximum difference between the simulation and experiment results are 5.35% and 3.32%, respectively. It is evident that the CFD/CSD simulation results are in consistency with both wind tunnel experiment and commercial software results.
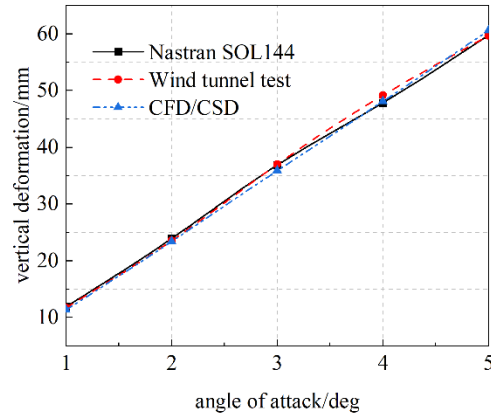
Figure 10: Comparison of test and simulation results of wingtip vertical displacement under 19m/s with different angle of attacks

5 CONCLUSIONS

The paper established a mesurement and control system used for gound/wind tunnel testing of propeller-wing system. Sensors utilized for this system mainly includes force balances, pressure taps, strain gauges, fiber Bragg gratings, vibration accelerometers and optical tachometers. Ground tests were carried out in advance to check the reliability of the measurement system and sensor design, and results were verified using CFD method. Wind tunnel tests include propeller-rigid wing aerodynamic experiments, propeller-elastic wing aeroelastic experiments, clean wing experiments, wing pressure measuring experiments, etc. Through analyzing the experiment data and comparing the data with results from numerical simulation methods, effectiveness of the constructed mesurement and control system is verified. This system will be employed further in following experiments. What needs to be pointed out is that mesurement accuracy of the propeller rotation speed in this experiment was 0.1%, thus improvements are needed on the measurement method, in expectation of increasing the accuracy to above 0.05%.

REFERENCES

[1] van Arnhem, N. Unconventional Propeller Airframe Integration for Transport Aircraft Configurations[D]. Ph.D. Dissertation, Delft Univ. of Technology, Delft, The Netherlands, 2022.

[2] Zhang Z., Xie C., Huang K., et al. Influence of Aerodynamic Interaction on Performance of Contrarotating Propeller/Wing System[J]. Aerospace, 2022, 9(12): 813.

[3] Wang K., Zhou Z., Zhu X., et al. Aerodynamic Design of Multi-Propeller/wing Integration at Low Reynolds Numbers[J]. Aerospace Science and Technology, 2019, 84: 1-17.

[4] An S. Aeroelastic Design of a Lightweight Distributed Electric Propulsion Aircraft with Flutter and Strength Requirements[D]. Atlanta: Georgia Institute of Technology, 2015.

[5] Stoll A. M., Bevirt J., Moore M. D., et al. Fredericks, N. K. Borer. Drag Reduction Through Distributed Electric Propulsion[C]. AIAA Aviation, Atlanta, GA, 2014: AIAA-2014-2851.

[6] Nikolai H., Dennis K., Christian B. Two Aerodynamic Mid-Fidelity Approaches on a Distributed Propulsion Wing[J]. Journal of Aircraft, 2024, 61(1):196-210.

[7] Teixeira P. C., Cesnik C. E. S. Propeller Effects on the Response of High-Altitude Long-Endurance Aircraft[J]. AIAA Journal, 2019, 57(10):4328-4342.

[8] Michael D. P., Matthew J. D. Conceptual Design of Electric Aircraft with Distributed Propellers: Multidisciplinary Analysis Needs and Aerodynamic Modeling Development[C]. 55th AIAA Aerospace Sciences Meeting, National Harbor, Maryland, 2014: AIAA-2014-0534.

[9] Joaquin E., Bernardo P., Shugo K., et al. Rapid Aerostructural Optimization of Wing-Propeller Systems[C]. AIAA SciTech 2024 Forum, Orlando, FL, 2024: AIAA-2024-0374.

[10] Brian J. G., Mark F. R. Experimental Analysis of Propeller-Wing Interactions for a Micro Air Vehicle[J]. Journal of aircraft, 2009, 46(1), 1-9.

[11] Zhang X., Zhang W., Li W., et al. Experimental research on aero-propulsion coupling[J]. Chinese Journal of Aeronautics, 2023, 36(2), 201-212.

[12] Shreyas S. and Juergen R. (2023). Wind Tunnel Measurements of Propeller-Wing Interactional Aerodynamics[C]. AIAA AVIATION 2023 Forum, San Diego, CA and Online, 2023: AIAA-2023-3542.

[13] Meng Y., Wan Z., Xie C., et al. Time-domain nonlinear aeroelastic analysis and wind tunnel test of a flexible wing using strain-based beam formulation[J]. Chinese Journal of Aeronautics, 2021, 34(1):380-396.

[14] Meng Y., Xie C., Wan Z. Deformed wing shape prediction using fiber optic strain data. 17th international forum on aeroelasticity and structural dynamics, 2017.

COPYRIGHT STATEMENT